FNAL TD Note # TD-06-041

July 2006, last revision August 09, 2006

SS-I Section Focusing Solenoid Prototype Cold Mass Design

G. Davis, V.V. Kashikhin, T. Page, I. Terechkine, T. Wokas

I. The solenoid requirements

A set of requirements for the solenoid has been developed as a result of several iterations of making magnetic design, simulating beam dynamics, and finalizing the acceleration section layout (Table 1).

Table 1: SS-I Section Focusing Solenoid

Number of solenoids in the section	18
Parameter	
Bore diameter (mm)	30
Bore type	cold
Integrated Strength ($T^2 \cdot mm$)	3000
Field margin	30%
Field strength at 200 mm from the solenoid center (Gs)	< 1.0
Acceptable cold mass length (mm)	220
Available insertion gap (mm)	250

The integrated strength in the table is defined as $IS = \int_{-\infty}^{+\infty} B_z^2 dz$

As it was in the case of the CH-type cavity section [1], the requirement of having limited axial extension of the magnetic field resulted in a necessity of using bucking coils to direct the magnetic flux into the external flux return. If superconducting cavities are used for acceleration, this requirement is especially important because with each quench in the cavities, the residual magnetic field penetrates the cavity walls introducing zones with "normal" conductivity resulting in degradation of the cavity quality factor. It would take warm-up of the cavities to reset the quality factor to its initial value. The desired level of magnetic field on the walls of cavities depends on the design quality factor and quality of Niobium used for fabrication; usually it is of the order of 1 μT or 10 mGs [2]. With the required solenoid bore and integrated strength, it is not possible to achieve this low fringe field directly. So, after using the bucking coils to reduce the fringe field to the level of the order of the earth field of ~1 Gs, one need an additional shielding that would bring the residual field to the needed level.

This note describes the status of the solenoid cold mass design and serves as a design proposal **for the Type I Single Spoke Cavity Section Focusing Solenoid** stating the parameters we are aiming to reach. Although it is quite possible that more changes will be made to the design, at the moment those changes do not seem significant to us. Because eliminating magnetic field on cavity walls becomes very important, issues associated with imperfectness of the assembly (including uncertainty of the packing factor) and hysteretic properties of the strand, which result in the dependence of the fringe field on the magnet excitation history, must be investigated. Effectiveness of additional magnetic screening must also be evaluated to provide initial input for the magnetic shielding design.

II. Magnetic Design

Current magnetic design is based on the next set of winding parameters:

- the main coil is wound using **an ML-insulated, round 0.808 mm SSC strand** with **0.1 mm thick insulation** between the layers of winding;
- the bucking coils are wound using round insulated **0.5 mm** Oxford strand with **0.1 mm insulation** between the layers of winding.

Parameters of strand used during modeling and main modeling results for the prototype solenoid (ideal set of parameters) are shown in tables 2 and 3. Values of compaction factors rely of results obtained while the practice coils and the test solenoids [3] were fabricated and depend on the choice of strands and insulating materials.

Table 2. Strand parameters.

Parameter	Unit	Main	Bucking
Bare (round) strand diameter	mm	**0.808**	**0.500**
Strand insulation thickness	mm	**0.025**	**0.020**
Copper to non-copper ratio	-	**1.5**	**1.35**
Non-Cu critical current density at 5 T, 4.2 K	A/mm^2	**2750**	**2750**
Engineering current density at 1 A current	A/mm^2	**1.4383**	**-3.4673**

Table 3. Solenoid parameters at 4.2K.

Parameter	**Unit**	**Value**
Coil aperture	mm	**40**
Number of turns in the main coil	-	**166x29**
Number of turns in the bucking coils	-	**2x10x44**
Average strand packing factor in the main coil	-	**0.74**
Average strand packing factor in the bucking coils	-	**0.68**
Yoke length	mm	**186**
Parameters at FI = 300 T^2cm		
Magnet current	A	**133.53**
Central field, B_0	T	**5.406**
Peak field in the coil, B_{peak}	T	**5.465**
Field integral	T^2cm	**300.00**
Effective length, L_{eff}	mm	**122.13**
Field integral ratio over $2L_{eff}$	%	**99.98**
Peak radial field at 10 mm off the axis	T	**0.74**
Stored energy	kJ	**3.764**
Magnet inductance	H	**0.422**
Parameters at quench		
Magnet current	A	**204.2**
Central field, B_0	T	**8.265**
Peak field in the coil, B_{peak}	T	**8.355**
Field integral, *FI*	T^2cm	**700**
Peak radial field at 10 mm off the axis	T	**1.13**
Stored energy	kJ	**8.8**
Axial force per bucking coil	kN	**33**

A series of figures below show the current magnetic design layout, solenoid load curves with strand critical surfaces, and the longitudinal profile of the magnetic flux density.

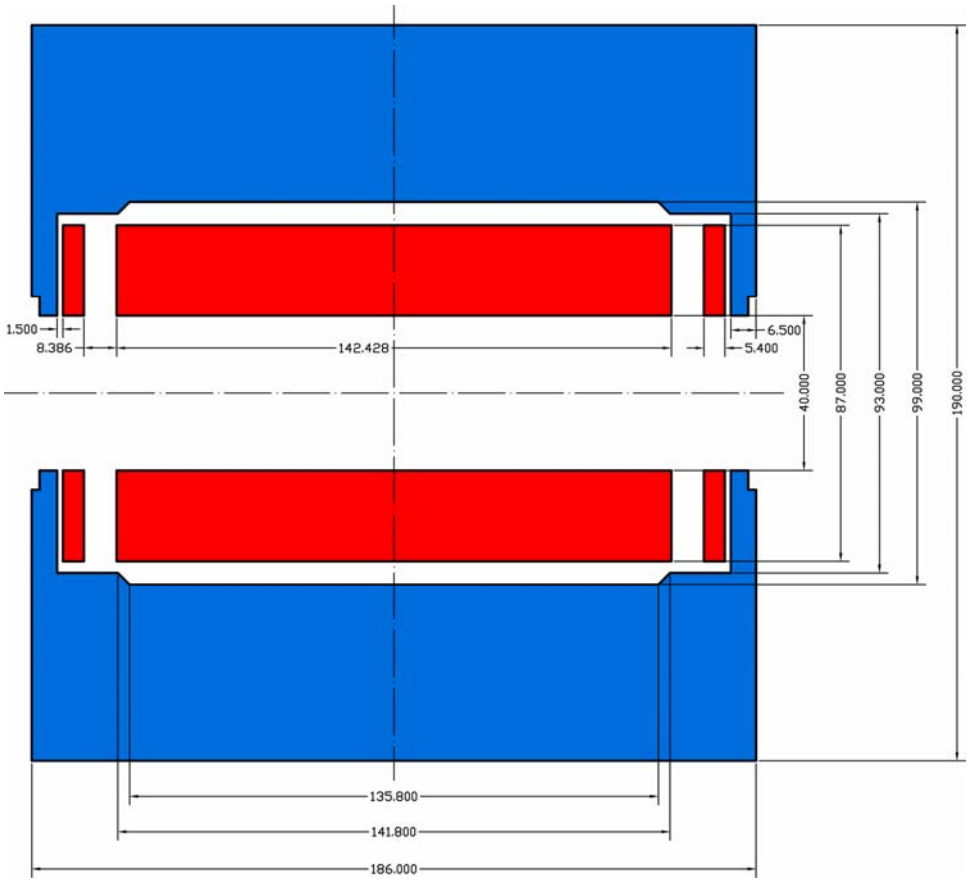

Fig. 1. SSR-I section solenoid cold mass layout

Load curves for the main and bucking coils are shown with the critical surfaces of the used superconducting strand @ 4.2 K:

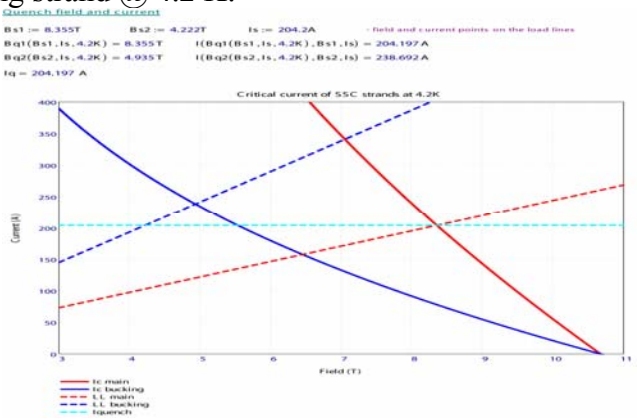

Fig. 2. Critical current diagram

Onset of quench for bucking coil happens at higher current than for the main coil.

Longitudinal distribution of the axial magnetic filed along the axis is shown in Fig. 3, where distance is in “mm” and field is in “Tesla”.

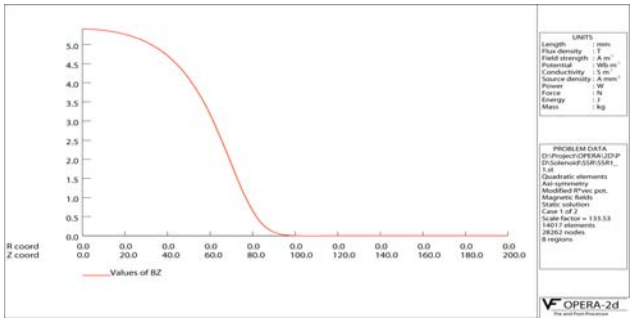

Fig. 3: Axial magnetic field along the axis of the solenoid

It is possible to note quick decay of the residual field outside of the solenoid as a result of compound action of the bucking coils and the flux return. Nevertheless, as it was mentioned above, the design does not allow reduction of fringe magnetic field to the level significantly below 0.5 Gs (50μT) as the graph in Fig. 4 shows.

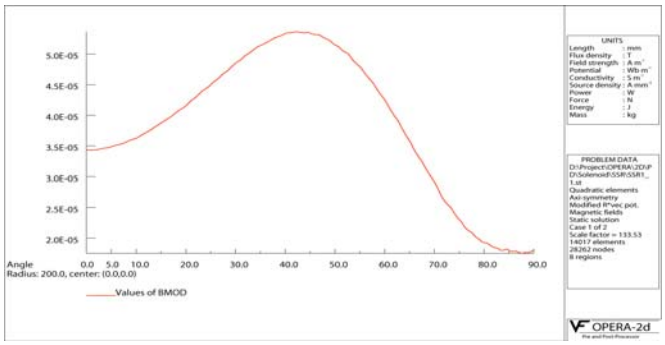

Fig. 4: Magnetic filed at the distance 200 mm from the center of the solenoid

Magnetic field on the cavity wall (located ~ 240 mm from the center of the solenoid, as Fig. 9 below shows) depends on factors like precision of fabrication, hysteretic properties of strand, and magnetic properties of material used to build the solenoid flux return. Impacts of these factors will be analyzed in this note.

Radial component of magnetic field (in Tesla) at maximal current along the line parallel to the axis at the distances 10 mm from the axis is shown in Fig. 5. It is important for this component of the magnetic field to be kept at a reasonably low level to prevent stripping of H^- ions accelerated in the linac. In this case, estimate of the effect gives encouraging result of low stripping loss.

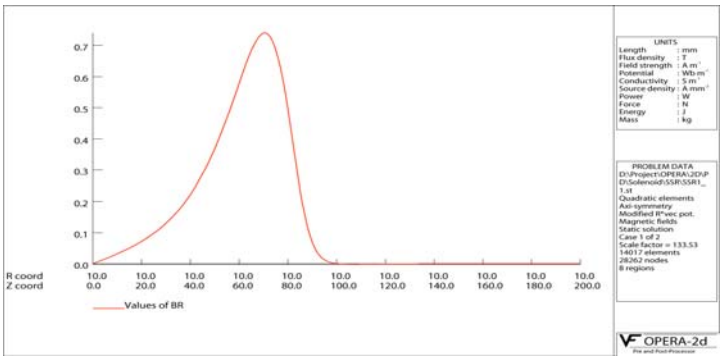

Fig. 5: Radial magnetic field along the axis at the distance of 10 mm from the axis

III. Mechanical Design

The value of the axial force of ~ 33 kN applied to the bucking coils (see Table 3), is high enough to require certain measures to prevent movement of the coils. As it was in the case of the CH-type section solenoid [1], pre-stress of the coil assembly combined with the pre-tension of the cryostat inner pipe (which in this case serves simultaneously as a beam pipe) can help to limit movement of the solenoid bucking coil to the desired level. The proposed design concept of the solenoid is shown in Fig. 5 below:

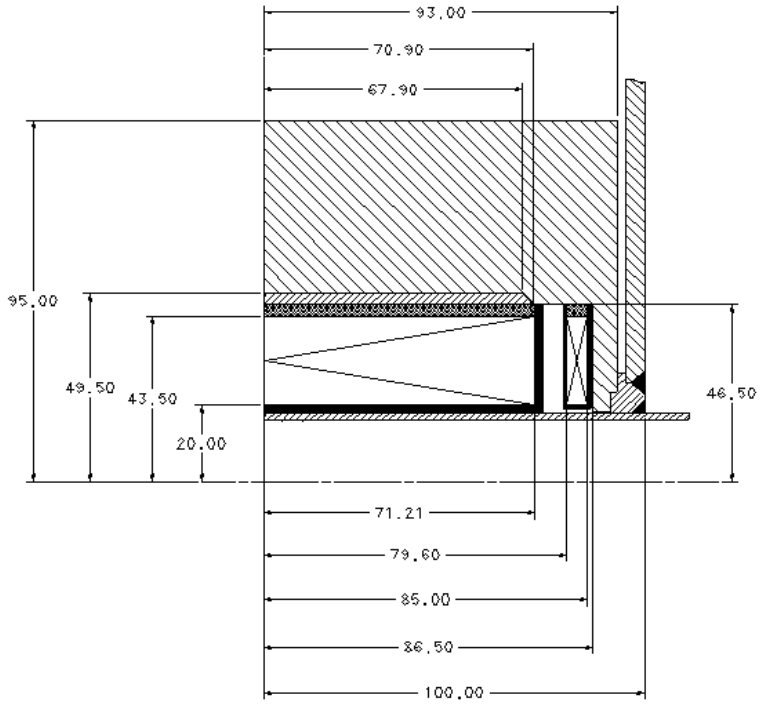

Fig. 5: Solenoid design concept

Main geometry features agree with what is shown in Fig. 1. Without taking measures to restrict coil movement, deformation in the ends of the flux return exceeds 50 μm and stress exceeds soft steel elasticity limit. Additional support is provided during assembly by welding a pre-stress ring to the pipe, which is stretched by using special tooling; similar method was used for the CH-type section solenoid [1]. Additional force of ~10 kN applied inward to the inner end of the flux return flange is required to bring the bucking coil displacement (or deformation of the end walls of the flux return) to the level of ~ 15 μm, which seems acceptable. Illustrating diagrams are similar to those shown in [1] and are not shown here.

Because the inner diameter of the LHe vessel pipe is smaller than in the case of the CH-type section solenoid, it appeared difficult to use exactly the same technique to stretch the pipe; instead, slightly different way of doing the stretching has been proposed. As it was made before, the inner surface of the pipe has a profile that allows application of pulling force, which is now generated by several tensioning bolts between a slotted puller and a clamp flange (Fig. 6).

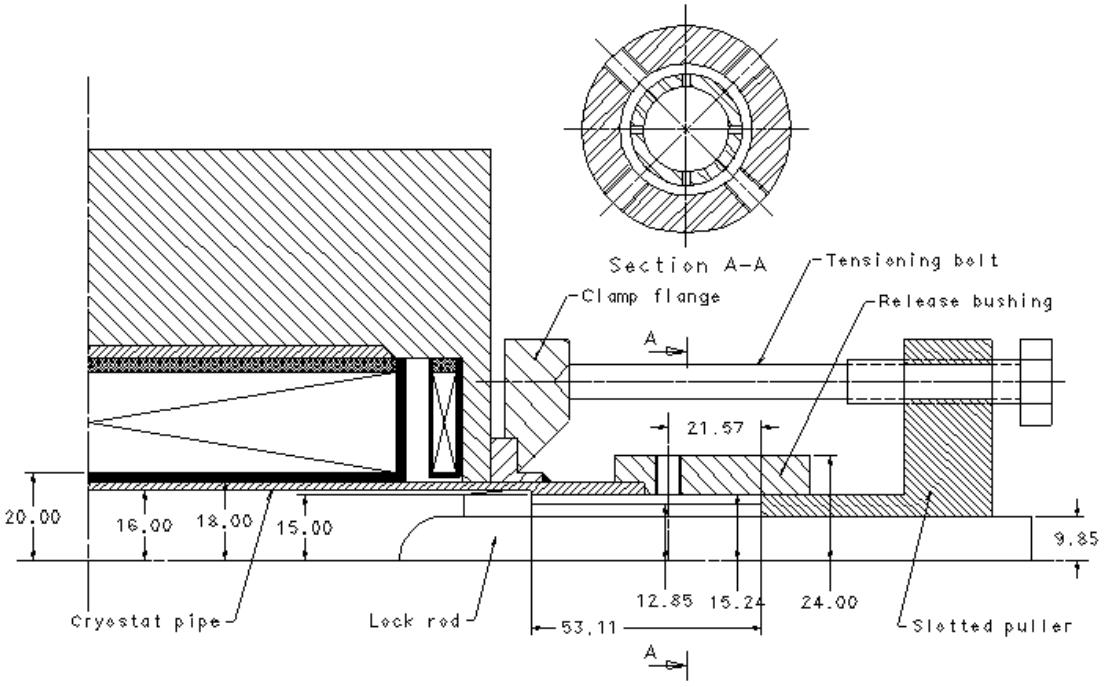

Fig. 6: Solenoid assembly tooling

The slotted puller is made of spring steel so that it could be inserted inside the pipe by applying axial force. To lock the puller inside the pipe, a lock rod is inserted inside the puller. After the tension is applied by using the tensioning bolts, the pipe is stretched and the solenoid assembly is compressed. At this moment, welding can be made to permanently attach the pre-stress ring to the pipe. To remove the stretching tooling after the seal is cooled down, one need to release tensioning bolts, remove lock rod, and use release screws with the release bushing to push inward fingers of the slotted puller until it can be safely removed from the inside of the pipe. The same bushing can be used to insert the puller inside the pipe instead of snapping it in place by using longitudinal force.

If dimensions of the beam pipe (made of 316 stainless steel) are as shown in Fig. 6, elasticity coefficient, that binds the pipe stretching with applied force, k1 = 2.5 μm/N. The elasticity coefficient of the assembled solenoid under compression can be found by modeling: k2 = 0.3 μm/N. Because k2 << k1, after removing the stretching tooling the pipe looses only about 20% of its tension, so, the goal stretching force is ~ 12 kN that must be ensured by an appropriate choice of the torque for the tensioning bolts.

To remove the slotted puller after pre-stress is applied, one must push fingers of the slotted puller. Required force is defined by the length of the fingers and location of the point where the force is applied. For the geometry shown in Fig. 6, the outer diameter of the active part of the puller is 25.7 mm and wall thickness of this part is 3.0 mm. The force needed to release the puller is about 1000 N per 1 mm of the displacement of the lock, which sounds quite acceptable. To further reduce the required load, it is possible to reduce thickness of the puller or make fingers narrower. Hardware modeling is desired to make right choice here. Fig. 7 shows deformation plot of one of the fingers under the force of 1000 N

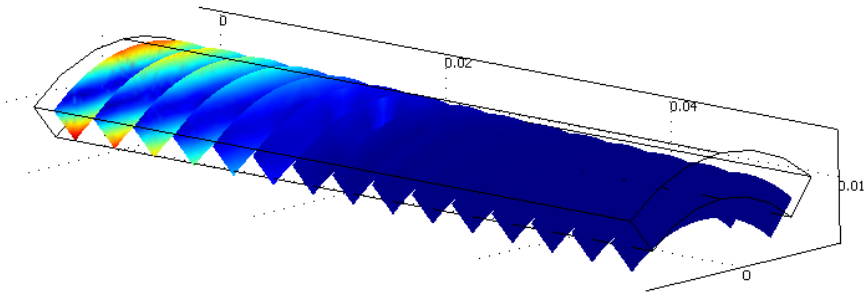

Fig. 7: Deformation of a finger under force of 1000 N. Deformation scale is 2:1.

Fig. 8 provides profile of the finger along it's length

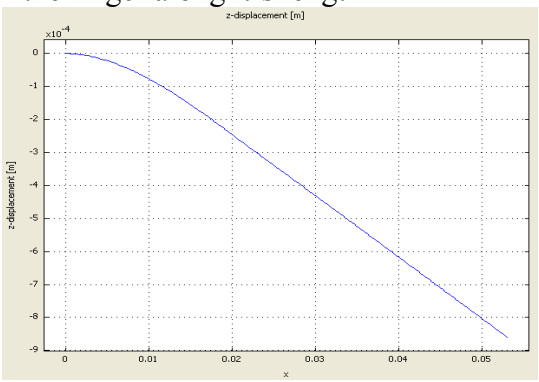

Fig. 8: Deformation of a finger of the puller as a function of its length

Maximal stress in the puller happens near the places where the fingers start and reach 1000 MPa, so proper steel choice should be made for the puller if it is desirable to make it reusable.

IV. Impact of uncertainties

Magnetic design for the SSC section focusing solenoid described above resulted in finding a solution that meets all major requirements except for the fringe field on the walls of superconducting cavities. To bring the fringe field to the level of 10 mGs (1 μT), additional shielding is needed. At this point, it is important to understand what can happen if design parameters of the solenoid deviate from their nominal values. Two things have high probability to happen:

1. Length of the main coil, or the bucking coil, or both of them can differ from their nominal values; distance between the coils can also change. If the coil packing factor is as expected, the coil thickness will also change if the nominal number of turns is wound. So, the profile of the magnetic field will change and so the fringe filed will do.

2. Packing factor can differ from what was expected. If the coil length is unchanged, thickness of the coil will change resulting in different fringe field.

A point on the cavity wall where fringe field must be closely watched can be found from the layout of the SSC section shown in Fig. 9 and Fig. 10 below [4].

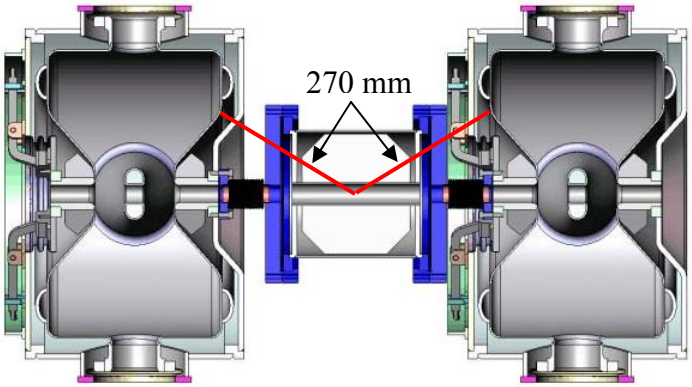

Fig. 9: Layout of the solenoid between the cavities in the SSC section

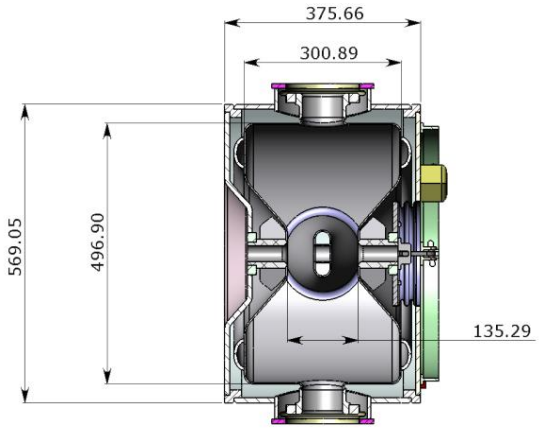

Fig. 10: Single spoke cavity

The nearest distance from the center of the solenoid to the cavity wall is ~ 270 mm; the coordinates of the nearest point are: r = 135 mm, z = 225 mm. Having this in mind, magnetic modeling was made to understand how deviations in the length of the coils in the solenoid and packing factors affect field in the nearest point on the cavity wall. The modeling was made using COMSOL software; some difference in comparison with the results presented earlier and obtained by using TOSCA package (Fig. 3 and Fig. 4) can be explained by difference in the representation of magnetization properties of the flux return. Fig. 11 shows change of the fringe field due to deviation in the coil length.

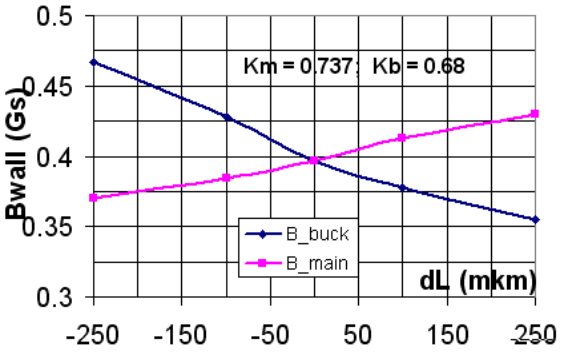

Fig. 11: Fluctuation of the fringe magnetic field due to deviation in the coil length

Here dL designates increase in the full length of each bucking coil or half of the length of the main coil. It is assumed that the position of the inner side of the bucking coil does not change. Although bobbin for each coil can be made quite precisely, during assembly and coil winding some fluctuations can take place. Experience of making the test coils proves that the main coil length can be made within 0.2 mm from the nominal size; for the half of the coil it means that $|dL| < 0.1$ mm. If to accept similar deviations in the full length of the bucking coils, we can talk about possible increase of the magnetic field on the wall by less than 0.05 Gs.

Fig. 12 shows how the wall field changes due to deviation in the coil packing factor.

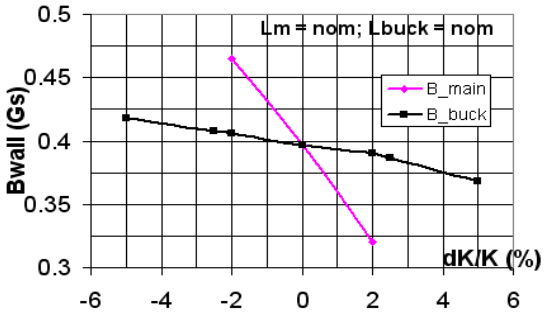

Fig. 12: Fluctuation of the fringe magnetic field due to deviation in the packing factor

If the length of the coil stays perfect, any changes in the packing factor results in corresponding change in the thickness of the winding, which results in some change of the fringe field. Experience of winding the practice and test coils shows that with the existing insulation material and with the winding made by one person (T. Wokas), we can talk about reproducibility of the packing factor for the coils with similar geometry (and wound using the same strand) within ~ +/- 2%. Most probably, for the bucking coils we will see less reproducible results. We will assume the packing factor reproducibility for the bucking coils of ~ +/- 5%. Change of the packing factors in the limits mentioned above results in the maximal fringe field change of less than 0.1 Gs.

Another geometrical parameter of the solenoid is distance between the main coil and the bucking coil, which is (nominal value) 8.386 mm. Although this distance can be changed by shimming by steps of ~50 μm, it would be useful to know sensitivity of the system to this shimming. Fig. 13 shows this graph. We can talk here about sensitivity of the fringe field to the gap change of less than 0.05 Gs per 100 μm. This is quite encouraging result that in principle can allow simplification of the coil assembly.

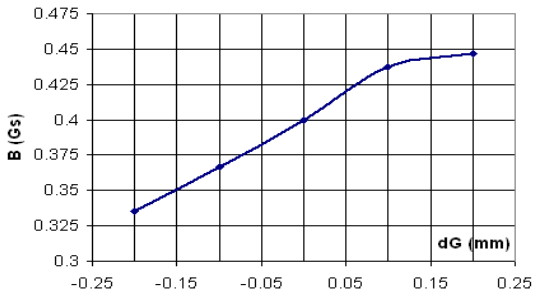

Fig. 13: Fringe field on the cavity wall at the nearest point as a function of a gap between the main coil and the bucking coil

Combined action of the three factors that were investigated above can be evaluated if one realizes that the sum of the three deviations: dLm + dLb +dG can be controlled by shimming. Fig. 14 shows how values of the fringe field at the surface of the cavity change if the total length of the solenoid is controlled within certain limits by shimming, allowing deviation in the lengths of the main coil and the bucking coils.

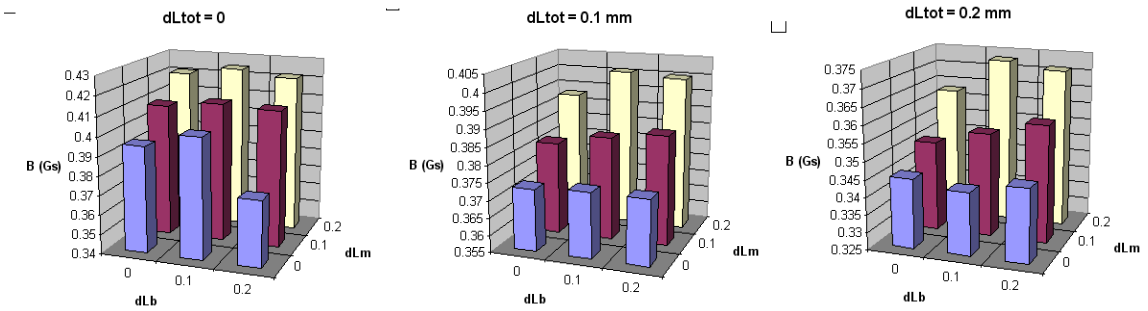

Fig. 14: Fringe field as a function of variation in the coil length and limited total length correction by shimming

For dLtot = 0 field can increase by ~ 0.04 Gs when the length of the main coil increases by 0.4 mm (length of one half of the main coil is shown in Fig. 14). That fact that one can get the fringe field lower than in the nominal case means that the magnetic design is not perfectly optimized. Allowing some increase in the solenoid length (dLtot = 0.1 mm and dLtot = 0.2 mm) can result even in lower fringe field. Because this result can depend on the quality of the flux return and because the saving is not significant, we will not attempt to design better system based on this result.

In all the cases above, the difference between the minimal and the maximal fringe field does not exceed 0.05 Gs. So, the conclusion for this chapter is that it is quite feasible to compensate for change in the coil length by shimming, but even without making any efforts to neutralize inaccuracy in the assembly, the fringe field increase is quite modest.

V. Impact of hysteretic effects

We saw that magnetic field on walls of cavities exceeds the required level; so additional shielding is needed. Before design of the shielding can start, one needs to know how hysteretic effects in the superconducting coil and in the steel yoke affect the fringe field and what remnant field one have when the solenoid current is brought to zero. Analysis performed in [5] has shown that the low carbon steel yoke effectively shunts magnetic flux generated by magnetized strands in the solenoid coils. Even if the strand with the effective filament diameter of ~ 70 μm is used for the coil winding, the residual magnetic flux density on the cavity walls does not exceed 0.025 Gs (without the flux return this field reaches ~ 10 Gs). The yoke itself can also have some residual magnetization, and corresponding magnetic field on the cavity walls stays below 0.1 Gs even if the yoke material coercive force was taken of the level of ~ 5 Gs (for soft steel it is ~ 0.5 Gs).

As a result of these findings, it is possible to conclude that when the solenoid current is made "zero", without additional shielding magnetic flux density on the cavity walls can be about 0.1 Gs. If testing the prototype proves it true, this information can help in finalizing shielding requirements for superconducting RF cavities.

Another conclusion can be made that the hysteretic effects in parts of the solenoid do not change much the fringe field of a hysteresis-free solenoid we studied above; so the magnetic shielding can be designed without taking into the account the solenoid hysteretic behavior.

VI. Magnetic shielding

Allowed magnetic field on the cavity wall depends on the required quality factor Q of the cavity. Due to surface defects, the surface RF resistance can not be made infinitely small; it is quite feasible though to have it on the level of ~ 20 nOhm [e.g. see p. 171 in [6]). Power loss due to trapped magnetic flux can be expressed in terms of an additional surface resistance (p. 174 in [6]):

$$R_{mag} = 0.3(\text{nOhm})*H_{ext}(\text{mOe})*\{f(\text{GHz})\}^{1/2}$$

At 325 MHz, we can get a 25% increase in the surface resistance ($\Delta R_{mag} \approx 5$ nOhm) if H_{ext}=30 mGs. Because we expect seeing values of fringe field on the cavity surface of ~0.5 Gs, it is obvious that some shielding is needed.

Design of a cryostat that contains the solenoids employs magnetic shielding that presumably shunts the external, "earth" magnetic field and brings the magnetic field inside the cryostat to the desired level of ~1 μT. So additional screening is needed for the solenoid so that the magnetic field on the cavity walls stays low. The goal of this chapter is to show that it is possible to build shielding that would allow bringing the fringe field to the needed low level. The final choice of material and configuration of the shielding will be made after the prototype solenoid is tested and its fringe field becomes known.

Based on the solenoid layout shown in Fig. 9, we can imagine a cylindrical shield around the solenoid with disc-type walls on both sides. The next dimensions of the shield are accepted for the initial estimate: the outer diameter is 400 mm, total length is 320 mm, diameter of a beam pipe bore in the walls is 60 mm, shield wall thickness is 1 mm, and permeability of the shielding material is ~5000.

It is necessary to take into the account that the initial permeability of the material must be high so that efficiency of the shield is not compromised at low field. For example, low carbon steel has the initial permeability of less than 1000 [7, p. 110], which is not quite enough for our purpose. On the contrary, initial permeability of Iron-Nickel alloys can reach 10,000 [7, p. 337] and even higher values [8]. Another concern is working temperature; the temperature of the shielding inside the cryostat is ~ 70 K. Some sources (e.g. [9]) provide data that show that for most of high-mu alloys permeability at the nitrogen temperature is ~0.1 of its initial value at room temperature. On the contrary, for specially designed alloy "Cryoperm-10", permeability is higher at low temperature (see Fig. 15 below).

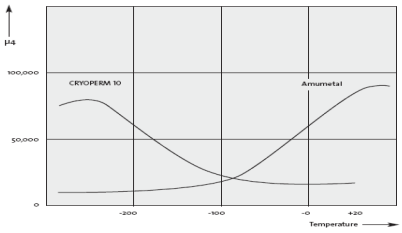

Fig. 15: Temperature dependence of permeability

The first thing to start with while designing shielding is to check what boundary conditions we are going to have for the system shown in Fig. 9. Because inside of the accelerating section cryostat is installed "global" magnetic shielding (outer radius ~ 450 mm), we will have here boundary condition with assigned (zero) magnetic potential; in the vicinity of this cylindrical boundary magnetic field lines are arranged in the radial direction. Somewhere inside cavities, in the mid-plane between the two solenoids, boundary condition will depend on how magnetic field vectors in the neighboring solenoids are arranges: parallel or anti-parallel. Fig. 16 below compares the two cases.

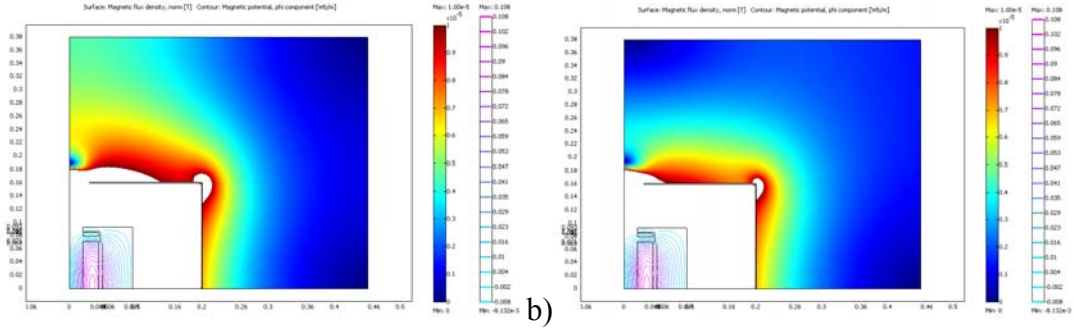

Fig. 16: Fringe field with parallel (a) and anti-parallel (b) direction of magnetic field in adjacent solenoids (μ = 5000).

It is possible to see that zone with higher field protrudes farther in the case when magnetic field vectors in the two solenoids have the same direction. In this case, on the cavity wall, the increase in the field is ~ 35%; for both cases the fringe field is higher than 30 mGs. The case with the field vectors oriented in opposite directions will be accepted for further analysis. Fig. 17 shows the fringe map and graph for μ = 10000.

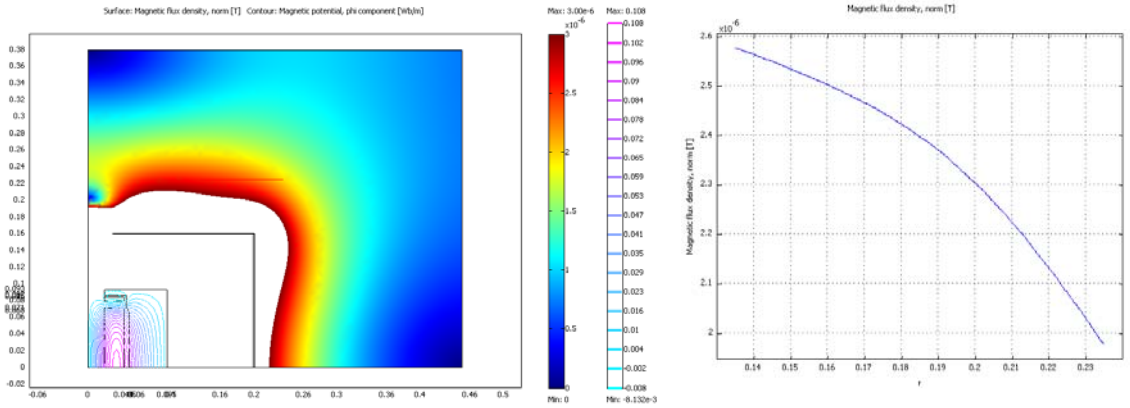

Fig. 17: Fringe field distribution with permeability of the screen $\mu = 10000$

With the shield walls thickness ~ 1mm and $\mu = 10000$, we marginally meet the condition $B < 3\mu T$, but questions remains on how well we know parameters of the flux return at LHe temperature. This issue is a subject for future study, and, unless we know magnetic properties of the flux return really well, we need to have significant reserve in the screening capacity of the shielding. To achieve the 10 mGs level, we need to use thicker material or materials with higher permeability; two-layer shielding [8] is also an option.

At the moment, the proposal is to build shielding using 1.5 mm (60 mil) thick Cryoperm@ sheet. The shielding must have several openings for current leads and He pipes. Each opening must be equipped with a Cryoperm@ shield of appropriate length. The whole shielding system must be well analyzed and the setup for the solenoid testing must allow measuring remaining fringe field inside a test cryostat.

At this point we just want to state that achieving fringe field of 1 μT seems not an easy task, although feasible with some attention devoted to details of the shielding.

VII. Conclusion remarks

Suggested design of a cold mass for the solenoid for the single spoke cavity section of the HINS linac meets the requirements with more that 50 % of reserve in the integrated strength. The device assembly technique has been suggested that allows application of a preload needed for compensation of electromagnetic forces.

Although testing the practice coils (PDST-01, -02, and 03 in [3]) provided quite encouraging information about the coil performance, some issues of the coil design will remain uncertain until the full cycle of the prototype solenoid fabrication and testing is completed.

The result of exercises performed above show that the solenoid fringe field does not critically change due to inevitable uncertainties in the solenoid parameters, whether these uncertainties are on the design level or acquired during fabrication.

Shielding cavities in the cryostat from magnetic field of solenoids appears not a trivial task taking into the account the desired level of fringe field. Nevertheless this can be made after proper investigation of the fringe field is made during testing of the prototype. Corresponding requirements for the solenoid test setup must be developed as soon as possible.

References:

1. G. Davis, et al, Linac CH-Type Cavity Section Focusing Solenoid Cold Mass Design, TD-06-020, FNAL, April 2006
2. A.W. Chao, M. Tigner, Handbook of Accelerator Physics and Engineering, p. 531
3. R. Carcagno, et al, Test Solenoids: Expected Performance and Test Results, TD-06-027, TD-06-028 and TD-06-029, FNAL, July 2006
4. G. Lafranco, Private communication
5. V.V. Kashikhin, I. Terechkine, Solenoid Residual Magnetization Study, TD-06-040, FNAL, July 2006
6. H. Padamsee, et al, RF Superconductivity for Accelerators, N-Y, 1998

7. David Jiles, Introduction to Magnetism and Magnetic Materials, Chapman & Hall, N-Y, 1998
8. W.G. Wadey, Magnetic Shielding with Multiple Cylindrical Shells, RSI, v. 27, 11, p. 910 – 916 (1956)
9. AMUNEAL corporation information: www.amuneal.com